Engineering of Hole Transporting Interface by Incorporating the Atomic-Precision Ag6 Nanoclusters for High-Efficiency Blue Perovskite Light-Emitting Diodes

Xue Bai (baix@jlu.edu.cn)
Jilin University

Fujun Zhang
State Key Laboratory of Integrated Optoelectronics, College of Electronic Science and Engineering, Jilin University

Yanbo Gao
State Key Laboratory of Integrated Optoelectronics, College of Electronic Science and Engineering, Jilin University

Po Lu
State Key Laboratory of Integrated Optoelectronics, College of Electronic Science and Engineering, Jilin University

Yuan Zhong
State Key Laboratory of Integrated Optoelectronics, College of Electronic Science and Engineering, Jilin University

Yue Liu
State Key Laboratory of Integrated Optoelectronics, College of Electronic Science and Engineering, Jilin University

Xinyu Bao
State Key Laboratory of Integrated Optoelectronics, College of Electronic Science and Engineering, Jilin University

Zehua Xu
State Key Laboratory of Integrated Optoelectronics, College of Electronic Science and Engineering, Jilin University

Min Lu
State Key Laboratory of Integrated Optoelectronics, College of Electronic Science and Engineering, Jilin University

Yanjie Wu
jilin university

Ping Chen
Jilin University

Junhua Hu
Key Laboratory of Materials Physics of Ministry of Education Department of Physics and Engineering,Zhengzhou University
Yu Zhang
Jilin University
Zhennan Wu
State Key Laboratory of Integrated Optoelectronics, College of Electronic Science and Engineering, Jilin University
Hongwei Song
Jilin university

Article

Keywords: Ag nanocluster, blue emission, hole transport layer, hole mobility, perovskite LEDs

Posted Date: September 2nd, 2022

DOI: https://doi.org/10.21203/rs.3.rs-2001366/v1

Abstract

The property of the underlying hole transport layer (HTL) plays a crucial role in determining the optoelectronic performance of perovskite light-emitting devices (PeLEDs), as their governing abilities in carrier injection and charge transport. However, endowing the current HTL system with a deep highest occupied molecular (HOMO) level concurrent with high hole mobility is still a big challenge, in particular being an open constraint toward high-efficiency blue (range of 460–495 nm) PeLEDs. In this regard, employing the traditional HTL material of poly(9-vinylcarbazole) (PVK) as a model, we perform efficient incorporation of the atomic-precision metal nanoclusters (NCs), [Ag_6PL_6, PL = (S)-4-Phenylthiazolidine-2-thione], to achieve significant tailoring in both of HOMO energy level (from − 5.8 eV to -5.94 eV) and hole mobility from (2.5×10^{-5} to 2.34×10^{-4} cm^2 V^{-1} s^{-1}), thus realizing the flat-band injection of holes between HTL and emitting layer and a strengthened ability in hole transport. As a result, the as-modified PeLEDs exhibit an external quantum efficiency (EQE) of 12.02% at 488 nm, which is around 1.3 times higher than that of the control device, i.e., 9.48%. The presented study exemplifies the success of metal NCs involved in HTL engineering by deepening the concept of the metallic molecule, and offers a simple while an effective additive strategy to settle the blue PeLEDs HTL dilemma, which paves the way for the fabrication of highly efficient blue PeLEDs.

1. Introduction

The properties of the underlying hole transport layer (HTL) in perovskite light-emitting devices (PeLEDs) play a key role in determining optoelectronic performance by affecting carrier charge transport and injection.[1–5] An ideal HTL should possess multiple functions of efficient hole injection and transportation as well as electron blocking, which requires deep highest occupied molecular (HOMO) energy level and the high hole mobility of HTL materials. However, given the fact that the intrinsic p-i-n planar structure and the limitation in the fabrication process of PeLEDs, the lack of desired HTLs that meet such requirements still restricts the development of their device performance,[6–8] especially in the blue (range of 460–495 nm) PeLEDs where utilize a wide bandgap as the light-emitting layer.[9]

As to the HTLs, they could be roughly divided into three species: (1) Inorganic materials are the most commonly used HTL for PeLEDs due to their low cost, high carrier mobility, and good optical transparency. However, the fabrication of inorganic materials typically requires high-temperature and high-vacuum processes, which impede their application in large-area and flexible devices.[10,11]; (2) In parallel, organic materials used widely in the organic LEDs (OLEDs) have also been well-employed as HTLs for PeLEDs. On the contrary, organic materials-based HTLs enable device fabrication via solution processing at room temperature. However, the low glass transition temperature of organic small molecules makes them difficult to attain a high-quality film, decisive in the final performance of the device.[12]; (3) Compared with the above two HTLs materials, organic polymers are also the potential candidate for HTLs because of their better solubility in organic solvents, higher film quality, and suitability for the spin coating process.[13,14] When it comes to the blue PeLEDs, the polymer with the wide bandgap,

Poly(9-vinylcarbazole) (PVK), is a well-recognized HTL material.[15,16] Nevertheless, the HOMO of PVK is not deeper enough to close to the valence band maximum (VBM) of the perovskite emitting layer (EML), leading to a barrier for hole injection as well as substantial nonradiative recombination at the interface. In addition, the hole mobility of PVK is quite small (2.5×10^{-5} cm^2 V^{-1} s^{-1}), which restricts the hole transport. Therefore, it is highly desirable to dope the HTL material to adjust the hole transport and injection. To solve these problems, many additive materials have been developed to improve the property of HTL, such as adding small molecules and inorganic materials. Although small molecules can well enhance the hole injection of HTL, they show poor compatibility with perovskites as well as low conductivity.[17,18] In addition, inorganic materials with high hole mobility cannot tune the energy level alignment of HTL. The lower solubility of inorganic materials in organic solvent also results in poor HTL quality, which prevents their further development.[19,20] Therefore, there is an urgent need to develop additives, capable of simultaneously tuning the energy level alignment and enhancing the carrier transfer mobility to improve the HTL performance of blue PeLEDs.

Atomically precise metal nanoclusters (NCs), typically possess a sub-2-nm metal core consisting of a few to hundreds of metal atoms that are protected by an organic monolayer, and can be treated as metallic molecules as their integrated molecular- and metallic-like physicochemical properties, such as high electrical conductivity, abundant surface active sites, good solution processability, etc.[21,22] In this scenario, the NCs can interact with a variety of materials as electrodes sensitized materials, bifunctional interfacial mediator and photosensitizer, which has great application potential of being additives in the optimization of functional layers of photovoltaic devices.[23–25] Herein, considering the film formation process, stability, electrical conductivity, and energy level alignment, we employed the (S)-4-Phenylthiazolidine-2-thione (PL) capped Ag nanoclusters with a formula of $[Ag_6PL_6]$ as an additive to optimize the hole transport layer of PVK toward efficient blue PeLEDs.[26–28] Through the characterization of Kelvin Probe Force Microscopy (KPFM) and the density functional theory (DFT) calculations, the modulation of the energy level alignment by dipoles from Ag_6 NCs and PVK achieves the flat-band hole injection between the HTL and perovskite EML, reducing the turn-on voltage of the devices.[29–32] Meanwhile, the hole mobility of the PVK (2.5×10^{-5} cm^2 V^{-1} s^{-1}) is strengthened around 9.1-folds by Ag_6 NCs to 2.34×10^{-4} cm^2 V^{-1} s^{-1}, which results in balanced carrier transport realizing high device performance. The EQE of PeLEDs modified by Ag_6 NCs reached 12.02% and is around 1.3 times that of the control device (9.48%). In addition, the device-based Ag_6 NCs doping realized a higher luminance of 5554 cd/m^2 due to the more balanced carrier recombination.

2. Result And Discussion

Energy levels of the most commonly used polymer-hole transport materials are summarized and shown in Fig. 1a, which can be seen that PVK has become the most popular one for blue perovskite due to its deep HOMO energy level.[33,34] To further be suitable for the wide bandgap blue perovskite materials, atomically precise $[Ag_6PL_6]$ (Ag_6 hereafter) NCs were incorporated into the PVK HTL for PBA_2Cs_{n-}

$_1Pb_nBr_{3n+1}$ blue PeLEDs to improve device performance. The ultraviolet-visible (UV-vis) absorption spectrum of Ag_6 NCs dissolved in chlorobenzene (CB) with a band edge of 500 nm in Fig. 1b demonstrates that the Ag_6 NCs were successfully synthesized. The inset of Fig. 1b shows the molecule structure of monolayer-protected Ag_6 NCs which are composed of an octahedral Ag_6 framework and the ligand. The unique structure of Ag_6 NCs aids in improving Ag solubility in organic solvents, which expands the application of noble metal Ag with high conductivity and high mobility as a dopant in PeLEDs. The transmission electron microscopy (TEM) images of Ag_6 NCs in CB are shown in **Fig. S**1, implying that Ag_6 NCs have excellent monodispersity and the size distribution is around 2.4 nm. According to the ultraviolet photoelectron spectra (UPS) spectra and Tauc-plot shown in Fig. 1c and **Fig. S**2, the HOMO and lowest unoccupied molecular orbital (LUMO) energy levels of the Ag_6 NCs are calculated to be -6.29 eV, and − 3.45 eV, respectively. As shown in Fig. 1d, with the increase of the Ag_6 NCs content, the characteristic absorption intensity of the PVK in CB solvent at 400 nm related to the Ag_6 NCs increased, indicating that the Ag_6 NCs had been successfully mixed into PVK. Moreover, the scanning electron microscopy (SEM) and elemental mapping images of PVK films doped with 20% Ag_6 NCs show that all elements (C, N, Ag, and S) are uniformly distributed in the film, where S and Ag are characteristic elements of Ag_6 NCs, indicating that Ag_6 NCs have been successfully doped into PVK film (**Fig. S**3). In addition, the X-ray photoelectron spectroscopy (XPS) spectra of PVK films without and with Ag_6 NCs are shown in **Fig. S**4, a characteristic peak at 162.6 eV can be observed for the Ag_6 NCs modified PVK films, which is related to S from the Ag_6 NCs, indicating that Ag_6 NCs have been successfully doped into PVK films. (**Fig. S**4).[35,36]

The blue PeLEDs are fabricated with the device structure of glass/ITO/PEDOT: PSS/Poly[(9,9-dioctylfluorenyl-2,7-diyl)-alt-(4,4'-(N-(4-butylphenyl)] (TFB)/HTL/quasi-2D perovskite film /1, 3, 5-tris(N-phenylbenzimiazole-2-yl)benzene (TPBi)/(8-Quinolinolato)lithium (Liq)/Al, where PVK modified with Ag_6 NCs is used as the HTL. The schematic structure and cross-sectional SEM images of the device are shown in Fig. 2a, and the optimized thicknesses of PEDOT: PSS, TFB/PVK with Ag_6 NCs, quasi-2D perovskite of $PBA_2Cs_{n-1}Pb_nBr_{3n+1}$, TPBi, and Liq/Al layers are about 35, 20, 15, 50, and 100 nm, respectively. The normalized PL spectra of the perovskite film and the normalized electroluminescence (EL) spectra of devices without and with 20% Ag_6 NCs doping are shown in Fig. 2b. It is worth noting that the EL spectra are almost identical to the PL spectra, illustrating that luminescence derives from the perovskite ETL rather than other materials and the Ag_6 NCs do not affect the EL spectra. The EL emission peaks located in the blue region are at 488 nm with a narrow full-width at a half-maximum around 28 nm, which is consistent with PL spectra for the quasi-2D perovskite film. The EL spectra intensity of optimal and control devices gradually increases as the bias voltage increases from 4 to 7 V, as shown in Fig. 2c and **Fig. S5**, respectively, while the peak position remains unchanged indicating the great spectral stability of the devices. The current density-voltage-luminance intensity (J-V-L) curves and the EQE-current density (EQE-J) curves of the control device and the optimal device based on 20% Ag_6 NCs modified PVK are shown in Fig. 2d and e, respectively. The maximum luminance is obtained by the optimal device of 5554

cd/m^2, higher than that of the control device (2442 cd/m^2). The optimal device exhibits a maximum EQE of 12.02%, which is 1.3-folds higher than the control device (9.48%). In addition, further investigating the effect of the variation of Ag_6 NCs concentration on the device performance, the EQE of those devices increases as the content of Ag_6 NCs adds from 10–20% but drops sharply when the Ag_6 NCs content increases continuously to 30% (Table 1). Moreover, the current density at the same voltage shows an increasing tendency and the turn-on voltages of those devices gradually decrease, indicating that the Ag_6 NCs may increase carrier injection and transport ability to improve PeLEDs performance (**Fig. S6**). Device performance drop of the excessive Ag_6 NCs addition may result from the reducing the quality of perovskite films, which can be confirmed by the root mean square (RMS) of AFM images changing in the perovskite films on the modified PVK films (**Fig. S7**).

Table 1
Electronic performance of perovskite LEDs with 0–30% Ag_6 NCs doping in PVK.

HTL	FWHM (nm)	V_{on} (V)	L_{max} (cd/m^2)	EQE_{max} (%)
PVK	28	3.21	2442	9.48%
10% Ag_6 NCs	29	2.96	3265	10.40%
20% Ag_6 NCs	29	2.84	5554	12.02%
30% Ag_6 NCs	29	2.98	4240	11.22%

To elucidate the effect mechanism of Ag_6 NCs additives on device performance, the energy levels of the PVK without and with different concentrations of Ag_6 NCs films are explored by the UPS measurement and the Tauc-plots, and the corresponding results are shown in Fig. 3a and **Fig. S8**, respectively. It presents a decrease in the HOMO of PVK, from − 5.8 eV to -6.0 eV after the incorporation of Ag_6 NCs, indicating that the Ag_6 NCs can adjust the energy level of PVK. To investigate the influence of this change on the device performance enhancement, the conduction band minimum (CBM) and VBM of perovskite film are calculated by the absorption spectrum and UPS data (**Fig. S9**). As shown in Fig. 3b, it can be seen that the control device possesses a 0.15 eV potential barrier between PVK HTL and perovskite EML compared with the potential well between electron transport layer (ETL) and perovskite EML, which will cause inefficient hole injection and further affecting device efficiency. The 20% Ag_6 NCs doped into PVK can modify the HOMO energy level of PVK from − 5.8 eV to -5.94 eV approaching the EML VBM, which will achieve barrier-free hole injection to enhance the injection efficiency, reduce the annihilation of carriers at the interface between EML and HTL.[37–39] The energy level alignment changing may from two reasons, the surface potential changing or the stacking changes of the carbazole from the PVK by the effect of the Ag_6 NCs. The diffraction of x-rays (XRD) was measured for the ultrathin film PVK modified without and with Ag_6 NCs to explore the carbazole stack changes. As shown in **Fig. S10**, the grazing incidence XRD (GI-XRD) pattern gives detailed data about the PVK films with no change after the Ag_6 NCs

dopant suggesting the Ag_6 NCs do not influence the carbazole stack of the PVK.[40,41] The KPFM measurement shows that the surface potential of the PVK films modified by Ag_6 NCs has changed significantly, indicating that the band change may be due to the formation of dipoles between Ag_6 NCs and PVK (**Fig. S11**).[42–48] The effect of the Ag_6 NCs on the PVK film carrier transport is also further investigated, and the electrical conductivity (σ) of capacitor-like devices with the structure of ITO/HTL/Au is shown in Fig. 3c.[49] With the contents of Ag_6 NCs increasing from 10–30%, the calculated conductivities are 3.19×10^{-3} S cm^{-1}, 4.78×10^{-3} S cm^{-1}, and 6.54×10^{-3} S cm^{-1}, which are both higher than the pure PVK (2.2×10^{-3} S cm^{-1}), respectively, indicating that the electrical conductivity of the HTL strengthens gradually by doping Ag_6 NCs due to the metallic properties of Ag_6 NCs molecular states. The improved conductivity may be due to the increase in hole mobility, which is further demonstrated by the subsequent space-charge-limited-current region (SCLC) test. The hole mobility is calculated from the devices with the structure of ITO/PEDOT: PSS/HTL/Au (Fig. 3d).[50] The hole mobility of PVK with 10%, 20%, and 30% Ag_6 NCs films are 1.05×10^{-4} cm^2 V^{-1} s^{-1}, 2.34×10^{-4} cm^2 V^{-1} s^{-1}, and 3.57×10^{-4} cm^2 V^{-1} s^{-1}, which is higher than 2.5×10^{-5} cm^2 V^{-1} s^{-1} of the pure PVK films indicating that the Ag_6 NCs enhance the hole mobility. Summarizing the discussion above, the Ag_6 NCs as the dopant can enhance the hole injection and the transport by the modified HOMO energy level of PVK and its metallic properties, thereby enhancing device performance.

As mentioned above, we conclude that the reasons for the introduction of Ag_6 NCs to improve device performance are mainly divided into the following two aspects. As shown in Fig. 4a, the holes are rapidly transported through the acceleration of the Ag_6 NCs, thus compensating for the low hole mobility of PVK, forming a more balanced carrier transport. Meanwhile, the energy level of the PVK adjusts by the dipole that forms between the PVK and Ag_6 NCs, which is confirmed by the density functional theory (DFT) calculations. Figure 4b shows the electrostatic potentials (ESP) of the Ag_6 NCs and the PVK. The ESP for the complex model formed between the Ag_6 NCs and PVK is shown in Fig. 4c, and it can be seen that the Ag_6 NCs and PVK possess the respective negative and positive ESPs which interact with each other and form the dipole. Moreover, the HOMO energy level of modified PVK achieves barrier-free hole injection between HTL and EML, which will increase hole injection efficiency and promote the injection balance of electrons and holes. The accumulation of holes at the interface between EML and HTL will be suppressed which can be further manifested by the increase in device performance.

To explore the connection between the device performance enhancement and the unique structure of the Ag_6 NCs, ligands of Ag_6 NCs and the Ag nanoparticles (NPs) as the Ag_6 core analogs are used as additives for PVK to analyze the effect of various parts from Ag_6 NCs on device performance. The effect of the ligand and NPs on energy level alignment and the hole transport ability were investigated, respectively. Figure 5a and b show the UPS and hole mobility results of the PVK films with 5%, 10%, and 15% ligands doping. It can be seen that the HOMO energy level of those films is 5.82 eV, 5.85 eV, and 5.87 eV, and the conductivity of those films are 2.30×10^{-3} S cm^{-1}, 2.45×10^{-3} S cm^{-1}, and 2.61×10^{-3} S cm^{-1},

which shows insignificant change with PVK film indicating that may be mainly attributed to the fact that the ligands have little effect on the energy level alignment and hole mobility of PVK. The devices with different concentration ligands modified PVK HTL are fabricated with the same structure as the control device and the J-V-L and EQE-J curves of these devices are shown in **Fig. S12**. The current density curves of these devices at the same voltage and turn-on voltage are almost indistinguishable from the control devices, confirming that the ligands do not affect the hole injection and transport. Meanwhile, Fig. 5c shows the UPS spectra of the films with the different concentration Ag NPs indicating the Ag NPs with no ability to modify the suitable energy level alignment of the PVK like Ag_6 NCs. However, the conductivity of PVK films modified with 10%, 20%, and 30% Ag NPs are 3.19×10^{-3} S cm^{-1}, 4.87×10^{-3} S cm^{-1}, and 6.54×10^{-3} S cm^{-1}, respectively, which is higher than the PVK films suggesting the Ag NPs strengthen the conductivity of PVK. The devices with Ag NPs modified PVK HTL exhibits an increasing trend of current density at the same voltage with Ag NPs doping ratio adding but little change in the turn-on voltage with the doping ratio various, which confirms the Ag NPs possess the ability to enhance hole transport (**Fig. S13**). Moreover, the 10% Ag NPs modified device shows a higher EQE than the control device which may be attributed to the improved hole transport. However, the EQE sharply dropped with the Ag NPs doping contents further increasing from 10–30%. Further investigating the reason for EQE dropping, the AFM images of the PVK films with different concentrations of Ag NPs were measured and the responding results are shown in **Fig. S14**. The RMSs of PVK films are increased with the increase of Ag NPs doping content, indicating that doping Ag NPs reduced the quality of PVK films which is also proved by the leakage current increases with the concentration adding. Based on the above discussion, we confirmed the unique structure of the Ag_6 NCs is an important reason that it can improve device performance by enhancing the energy level alignment and mobility of HTL as an additive.

3. Conclusion

In conclusion, atomically precise Ag_6 NCs were successfully prepared and a mixture of Ag_6 NCs and PVK HTL was first utilized as the HTL for PeLEDs. On the one hand, barrier-free hole injection for the PeLEDs is achieved by adjusting the energy level alignment. On the other hand, the addition of Ag_6 NCs achieves charge carrier balance between ETL by enhancing the mobility of PVK HTL. As a result, a relatively high EQE of 12.02% was achieved by the device with 20% Ag_6 NCs doping, which is about 1.3 times higher compared with that of the control device (9.48%). Metal NCs as additives to modify the transport layer provide a new strategy to prepare suitable transport layers for wide-bandgap light-emitting materials and LEDs showing a great promise for applications in future display and lighting.

4. Materials And Methods

Materials

Dimethyl sulfoxide (DMSO, 99.99%) and chlorobenzene (CB, 99.99%) were purchased from Advanced Election Technology Co., Ltd. PEDOT: PSS (AI 4083) aqueous solution, 2,2’,2”-(1,3,5-Benzinetriyl)-tris(1-

phenyl-1-H-benzimidazole) (TPBi, 99.9%), Lead(II) bromide ($PbBr_2$, 99.99%), Phenylbutylamine bromide (PBABr, 99.9%), poly [9,9-dioctylfluoreneco-N-[4-(3-methylpropyl)]diphenylamine] (TFB), Poly(9-vinylcarbazole) (PVK), and (8-Quinolinolato)lithium (Liq, 99.9%) were purchased from Xi'an Polymer Light Technology Corp. (S)-4-Phenylthiazolidine-2-thione (99%), silver nitrate (99%), NaSCN (98%), ZnBr (98%), dodecane (99%), CH3COOAg (99%), 2-hexyldecanoic acid (99%), dimethylacet-amide (DMAc, 99%), acetonitrile (CH_3CN, 99%), acetic acid (99%), and oleylamine (80%) were purchased from Shanghai Aladdin Biochemical Technology Co., Ltd. All reagents were used as received without further purification.

Device fabrication

The indium tin oxide (ITO)-coated glass substrates were sequentially washed with water, ethanol, and acetone in sequence for 20 min and treated with O_3 plasma for 15 min. The PEDOT:PSS films were fabricated on the washed ITO by spin coating the PEDOT:PSS aqueous solution at the speed of 3000 rpm for 30 s and baked at 150°C for 30 min in ambient air. Then the TFB (in m-xylene, 8 mg ml^{-1}) was spin-coated on the top of PEDOT:PSS films at 2000 rpm for 60 s, followed by annealing on a hot plate at 120°C for 15 min in the glove box. The PVK (in CB, 10 mg ml^{-1}) or the modified PVK films were fabricated by spin-coated on the top of TFB films at 2000 rpm for 60 s, followed by annealing on a hot plate at 120°C for 15 min in the glove box.

The Ag_6 nanoclusters were prepared by dissolving (S)-4-Phenylthiazolidine-2-thione (0.1 mmol) and silver nitrate (0.1 mmol) into a mixed solvent of DMAc/CH_3CN (3:1), which evaporated slowly in darkness at room temperature for 2 days. Then the Ag nanocluster naturally dries and dissolves in chlorobenzene with stirring for more than 4 hours to accelerate dissolution The Ag nanoparticles were synthesized based on the method reported by Long Lin et al..[51]

The perovskite solution was fabricated by mixing the $PbBr_2$ (0.082 mmol), CsBr (0.08 mmol), PBABr (0.08 mmol), NaSCN (0.004 mmol) and $ZnBr_2$ (0.004 mmol) in 1mL of DMSO. Then the perovskite solution was spin-coated on the top of PVK films at 300 rpm for 5 s, 500rpm for 5 s, and 2500 rpm for 120 s, and after spin coating for 70 s, 100 µL ethyl acetate was immediately dropped onto the above film to template the crystallization of the perovskite crystals, followed by annealing on a hot plate at 55°C for 10 min. Finally, TPBi, Liq, and Al electrode layers were sequentially deposited by thermal evaporation (1×10^{-5} Torr).

Characterizations

Absorption and PL spectra were measured on Shimadzu UV-1900i spectrometer and Hitachi F-4700 spectrometer, respectively. TEM images were obtained on a JEM-2100F. SEM images and elemental mapping were collected on a JSM-7900F instrument. X-ray photoelectron spectroscopy (XPS) and ultraviolet photoelectron spectroscopy (UPS) were measured on an ESCALAB250 spectrometer. The roughness and the KPFM of the film were characterized by atomic force microscopy (AFM, Dimension Fastscan Bio, CA). The diffraction of X-rays (XRD) was conducted by using the grazing incidence (GI) mode in Rigaku Smartlab 9kw. The current density- voltage and luminance- voltage curves and the EL

spectra of the LEDs were collected on a Keithley 2400 sourcemeter and a PhotoResearch spectrometer PR650 with an adhesive encapsulation in the darkroom, respectively.

Density functional theory

The structure of Ag_6PL_6 was taken from the crystal structure in the literature, and the structure of PVK was constructed in which n = 5. The complex (i.e., Ag_6PL_6 mixed with PVK, PVK with Ag_6 NCs) formed between Ag_6PL_6 and PVK was also constructed. Then the geometry optimizations of Ag_6PL_6, PVK, and PVK with Ag_6 NCs were carried out by density functional theory (DFT) calculations using the Dmol^3 module[52] in the Materials Studio software package.[53] The Perdew-Burke-Ernzerh of (PBE)[54] modification of the generalized gradient approximation (GGA)[55] with the Grimme[56,57] custom method for DFT-D correction together with the doubled numerical basis set (DN) were used. The core electrons were treated by all electrons, and a global orbital cutoff of 3.4 Å and a Fermi smearing of 0.005 Ha were used for the optimizations. The convergence criteria include a self-consistent field (SCF) tolerance of $1.0 \cdot 10^{-4}$ Ha per atom, a maximum force tolerance of 0.004 Ha Å^{-1}, an energy tolerance of $2.0 \cdot 10^{-5}$ Ha per atom, and a maximum displacement tolerance of 0.005 Å were employed.

Declarations

Acknowledgements

F. Z. and Y. G. contributed equally to this work. The authors gratefully acknowledge the financial support from the National Natural Science Foundation of China (U21A2068, 11974142, 12104178, 61935009, 12174151), National Key R&D Program of China (2021YFB3500400), Science and Technology Development Program of Jilin Province (20200401059GX), the Natural Science Foundation of Jilin Province (20190201307JC).

References

1. Pham HD, Xianqiang L, Li W, Manzhos S, Kyaw AKK, Sonar P. Organic interfacial materials for perovskite-based optoelectronic devices. Energy Environ Sci 2019; 12: 1177–1209.
2. Li Z, Chen Z, Yang Y, Xue Q, Yip H-L, Cao Y. Modulation of recombination zone position for quasi-two-dimensional blue perovskite light-emitting diodes with efficiency exceeding 5%. Nat Commun 2019; 10: 1027.
3. Jeong J, Park JH, Jang CH, Song MH, Woo HY. Multifunctional Charge Transporting Materials for Perovskite Light-Emitting Diodes. Adv Mater 2020; 32: 2002176.
4. Han T, Tan S, Xue J, Meng L, Lee J, Yang Y. Interface and Defect Engineering for Metal Halide Perovskite Optoelectronic Devices. Adv Mater 2019; 31: 1803515.
5. Xue D-J, Hou Y, Liu S-C, Wei M, Chen B, Huang Z et al. Regulating strain in perovskite thin films through charge-transport layers. Nat Commun 2020; 11: 1514.

6. Zhang J, Wang L, Zhang X, Xie G, Jia G, Zhang J et al. Blue light-emitting diodes based on halide perovskites: Recent advances and strategies. Materials Today 2021; 51: 222–246.
7. Pan J, Quan LN, Zhao Y, Peng W, Murali B, Sarmah SP et al. Highly Efficient Perovskite-Quantum-Dot Light-Emitting Diodes by Surface Engineering. Adv Mater 2016; 28: 8718–8725.
8. Fakharuddin A, Gangishetty MK, Abdi-Jalebi M, Chin S-H, bin Mohd Yusoff AbdR, Congreve DN et al. Perovskite light-emitting diodes. Nat Electron 2022. doi:10.1038/s41928-022-00745-7.
9. Kang S, Jillella R, Jeong J, Park Y-I, Pu Y-J, Park J. Improved Electroluminescence Performance of Perovskite Light-Emitting Diodes by a New Hole Transporting Polymer Based on the Benzocarbazole Moiety. ACS Appl Mater Interfaces 2020; 12: 51756–51765.
10. Liu Y, Zhang L, Chen S, Liu C, Li Y, Wu J et al. Water-Soluble Conjugated Polyelectrolyte Hole Transporting Layer for Efficient Sky-Blue Perovskite Light-Emitting Diodes. Small 2021; 17: 2101477.
11. Shi Y-L, Zhuo M-P, Fang X-C, Zhou X-Q, Wang X-D, Chen W-F et al. Efficient All-Inorganic Perovskite Light-Emitting Diodes with Cesium Tungsten Bronze as a Hole-Transporting Layer. J Phys Chem Lett 2020; 11: 7624–7629.
12. Ho MD, Kim D, Kim N, Cho SM, Chae H. Polymer and Small Molecule Mixture for Organic Hole Transport Layers in Quantum Dot Light-Emitting Diodes. ACS Appl Mater Interfaces 2013; 5: 12369–12374.
13. Lu Y, Wang Z, Chen J, Peng Y, Tang X, Liang Z et al. Tuning hole transport layers and optimizing perovskite films thickness for high efficiency $CsPbBr_3$ nanocrystals electroluminescence light-emitting diodes. Journal of Luminescence 2021; 234: 117952.
14. Huang C-F, Keshtov ML, Chen F-C. Cross-Linkable Hole-Transport Materials Improve the Device Performance of Perovskite Light-Emitting Diodes. ACS Appl Mater Interfaces 2016;: 6.
15. Yuan S, Han B, Fang T, Shan Q, Song J. Flat, Luminescent, and Defect-Less Perovskite Films on PVK for Light-Emitting Diodes with Enhanced Efficiency and Stability. ACS Appl Electron Mater 2020; 2: 3530–3537.
16. Tria MC, Liao K-S, Alley N, Curran S, Advincula R. Electrochemically crosslinked surface-grafted PVK polymer brushes as a hole transport layer for organic photovoltaics. J Mater Chem 2011; 21: 10261.
17. Mali SS, Patil JV, Steele JA, Rondiya SR, Dzade NY, Hong CK. Implementing Dopant-Free Hole-Transporting Layers and Metal-Incorporated $CsPbI_2Br$ for Stable All-Inorganic Perovskite Solar Cells. ACS Energy Lett 2021; 6: 778–788.
18. Li J, Liang Z, Su Q, Jin H, Wang K, Xu G et al. Small Molecule-Modified Hole Transport Layer Targeting Low Turn-On-Voltage, Bright, and Efficient Full-Color Quantum Dot Light Emitting Diodes. ACS Appl Mater Interfaces 2018; 10: 3865–3873.
19. Liu G, Liu Z, Wang L, Xie X. An organic-inorganic hybrid hole transport bilayer for improving the performance of perovskite solar cells. Chemical Physics 2021; 542: 111061.
20. Wu Y, Xiao Z, He L, Yang X, Lian Y, Li G et al. Widely applicable phosphomolybdic acid doped poly(9-vinylcarbazole) hole transport layer for perovskite light-emitting devices. RSC Adv 2019; 9: 30398–

30405.

21. Zhou M, Jin R, Sfeir MY, Chen Y, Song Y, Jin R. Electron localization in rod-shaped triicosahedral gold nanocluster. Proc Natl Acad Sci USA 2017; 114. doi:10.1073/pnas.1704699114.
22. Zhou M, Zeng C, Sfeir MY, Cotlet M, Iida K, Nobusada K et al. Evolution of Excited-State Dynamics in Periodic Au_{28}, Au_{36}, Au_{44}, and Au_{52} Nanoclusters. J Phys Chem Lett 2017; 8: 4023–4030.
23. Guo P, Zhu H, Zhao W, Liu C, Zhu L, Ye Q et al. Interfacial Embedding of Laser-Manufactured Fluorinated Gold Clusters Enabling Stable Perovskite Solar Cells with Efficiency Over 24%. Adv Mater 2021; 33: 2101590.
24. Lee J, Naveen MH, Park J, Pyo K, Kim H, Lee D et al. Small Change, Big Difference: Photoelectrochemical Behavior of Au Nanocluster-Sensitized TiO_2 Altered by Core Restructuring. ACS Energy Lett 2021; 6: 2305–2312.
25. Abbas MA, Kamat PV, Bang JH. Thiolated Gold Nanoclusters for Light Energy Conversion. ACS Energy Lett 2018; 3: 840–854.
26. Han Z, Dong X-Y, Luo P, Li S, Wang Z-Y, Zang S-Q et al. Ultrastable atomically precise chiral silver clusters with more than 95% quantum efficiency. Sci Adv 2020; 6: eaay0107.
27. Kuznetsov AS, Tikhomirov VK, Shestakov MV, Moshchalkov VV. Ag nanocluster functionalized glasses for efficient photonic conversion in light sources, solar cells and flexible screen monitors. Nanoscale 2013; 5: 10065–10075.
28. Kang X, Li Y, Zhu M, Jin R. Atomically precise alloy nanoclusters: syntheses, structures, and properties. Chem Soc Rev 2020; 49: 6443–6514.
29. Chen Q, Wang C, Li Y, Chen L. Interfacial Dipole in Organic and Perovskite Solar Cells. J Am Chem Soc 2020; 142: 18281–18292.
30. LIU J-C, TANG F, YE F-Y, Qi C, CHEN L-W. Visualization of Energy Band Alignment in Thin-Film Optoelectronic Devices with Scanning Kelvin Probe Microscopy. Acta Phys -Chim Sin 2017; 33: 1934–1943.
31. Li C, Yang X, Zhao Y, Zhang P, Tu Y, Li Y. Hole extraction layer utilizing well defined graphene oxide with multiple functionalities for high-performance bulk heterojunction solar cells. Organic Electronics 2014; 15: 2868–2875.
32. Xiao X, Wang K, Ye T, Cai R, Ren Z, Wu D et al. Enhanced hole injection assisted by electric dipoles for efficient perovskite light-emitting diodes. Commun Mater 2020; 1: 81.
33. Zheng L, Zhai G, Zhang Y, Jin X, Gao L, Yun Z et al. Solution-processed blue quantum-dot light-emitting diodes based on double hole transport layers: Charge injection balance, solvent erosion control and performance improvement. Superlattices and Microstructures 2020; 140: 106460.
34. Wang W, Wu Z, Ye T, Ding S, Wang K, Peng Z et al. High-performance perovskite light-emitting diodes based on double hole transport layers. J Mater Chem C 2021; 9: 2115–2122.
35. Liu G, Liu Z, Wang L, Xie X. An organic-inorganic hybrid hole transport bilayer for improving the performance of perovskite solar cells. Chemical Physics 2021; 542: 111061.

36. Brown NMD, Cui N, McKinley A. An XPS study of the surface modification of natural MoS_2 following treatment in an RF-oxygen plasma. Applied Surface Science 1998; 134: 11–21.
37. Kim DB, Lee S, Jang CH, Park JH, Lee A, Song MH. Uniform and Large-Area Cesium-Based Quasi-2D Perovskite Light-Emitting Diodes Using Hot-Casting Method. Adv Mater Interfaces 2020; 7: 1902158.
38. Tanase C, Wildeman J, Blom PWM. Luminescent Poly(p-phenylenevinylene) Hole-Transport Layers with Adjustable Solubility. Adv Funct Mater 2005; 15: 2011–2015.
39. Zou C, Liu Y, Ginger DS, Lin LY. Suppressing Efficiency Roll-Off at High Current Densities for Ultra-Bright Green Perovskite Light-Emitting Diodes. ACS Nano 2020; 14: 6076–6086.
40. Bindumadhavan K, Roy S, Srivastava SK, Nayak BB. Synthesis and Characterization of Poly(N-vinylcarbazole)/Graphene Nanocomposites. j nanosci nanotechnol 2015; 15: 3733–3742.
41. Crispin X, Marciniak S, Osikowicz W, Zotti G, van der Gon AWD, Louwet F et al. Conductivity, morphology, interfacial chemistry, and stability of poly(3,4-ethylene dioxythiophene)–poly(styrene sulfonate): A photoelectron spectroscopy study. Journal of Polymer Science Part B: Polymer Physics 2003; 41: 2561–2583.
42. Sai N, Gearba R, Dolocan A, Tritsch JR, Chan W-L, Chelikowsky JR et al. Understanding the Interface Dipole of Copper Phthalocyanine (CuPc)/C_{60}: Theory and Experiment. J Phys Chem Lett 2012; 3: 2173–2177.
43. Zojer E, Taucher TC, Hofmann OT. The Impact of Dipolar Layers on the Electronic Properties of Organic/Inorganic Hybrid Interfaces. Adv Mater Interfaces 2019; 6: 1900581.
44. Maniadis P, Lookman T, Saxena A, Smith DL. Proposal for Manipulating Functional Interface Properties of Composite Organic Semiconductors with Addition of Designed Macromolecules. Phys Rev Lett 2012; 108: 257802.
45. Fukagawa H, Yamane H, Kera S, Okudaira KK, Ueno N. Experimental estimation of the electric dipole moment and polarizability of titanyl phthalocyanine using ultraviolet photoelectron spectroscopy. Phys Rev B 2006; 73: 041302.
46. Whitcher TJ, Wong WS, Talik AN, Woon KL, Rusydi A, Chanlek N et al. Energy level alignment of blended organic semiconductors and electrodes at the interface. Current Applied Physics 2018; 18: 982–992.
47. Ren Z, Xiao X, Ma R, Lin H, Wang K, Sun XW et al. Hole Transport Bilayer Structure for Quasi-2D Perovskite Based Blue Light-Emitting Diodes with High Brightness and Good Spectral Stability. Adv Funct Mater 2019; 29: 1905339.
48. Lin X, Jumabekov AN, Lal NN, Pascoe AR, Gómez DE, Duffy NW et al. Dipole-field-assisted charge extraction in metal-perovskite-metal back-contact solar cells. Nat Commun 2017; 8: 613.
49. Shen X, Zhang X, Wang Z, Gao X, Wang Y, Lu P et al. Bright and Efficient Pure Red Perovskite Nanocrystals Light-Emitting Devices via In Situ Modification. Adv Funct Materials 2022; 32: 2110048.

50. Ganzorig C, Sakomura M, Ueda K, Fujihira M. Current-voltage behavior in hole-only single-carrier devices with self-assembling dipole molecules on indium tin oxide anodes. Appl Phys Lett 2006; 89: 263501.
51. Synthesis, Growth Mechanism, and Characterizations. J Am Chem Soc 2018; 140: 17734–17742.
52. Delley B. From molecules to solids with the DMol(3) approach. J Chem Phys 2000; 113: 7756–7764.
53. DMol3 Module, MS Modeling, Version 2.2, Accelrys Inc., San, Diego, CA, 2003.
54. Perdew, Burke, Ernzerhof. Generalized Gradient Approximation Made Simple. Phys Rev Lett 1996; 77: 3865–3868.
55. Monkhorst HJ, Pack JD. Special points for Brillouin-zone integrations. Phys Rev B 1976; 13: 5188–5192.
56. Grimme S. Semiempirical GGA-type density functional constructed with a long-range dispersion correction. J Comput Chem 2006; 27: 1787–1799.
57. Grimme S, Antony J, Ehrlich S, Krieg H. A consistent and accurate ab initio parametrization of density functional dispersion correction (DFT-D) for the 94 elements H-Pu. J Chem Phys 2010; 132: 154104.

Figures

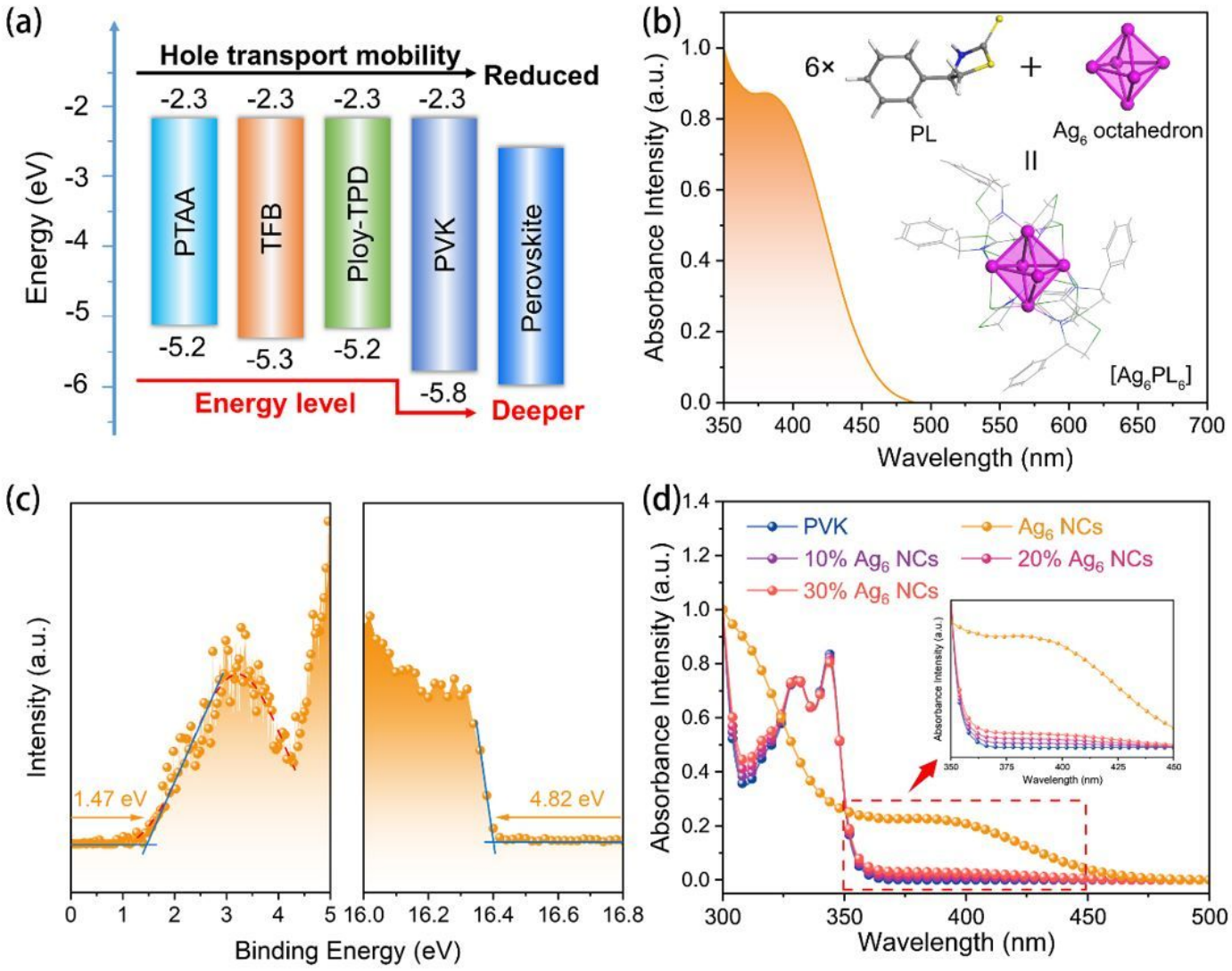

Figure 1

the energy level of the common-used polymer (a), the absorbance intensity curves of the Ag_6 NCs in CB (inset is the total structure of the $[Ag_6PL_6]$ NCs) (b), the UPS spectra of the Ag_6 NCs film (c) and the absorption spectra of PVK doped with different contents of Ag_6 NCs in CB solvent (d).

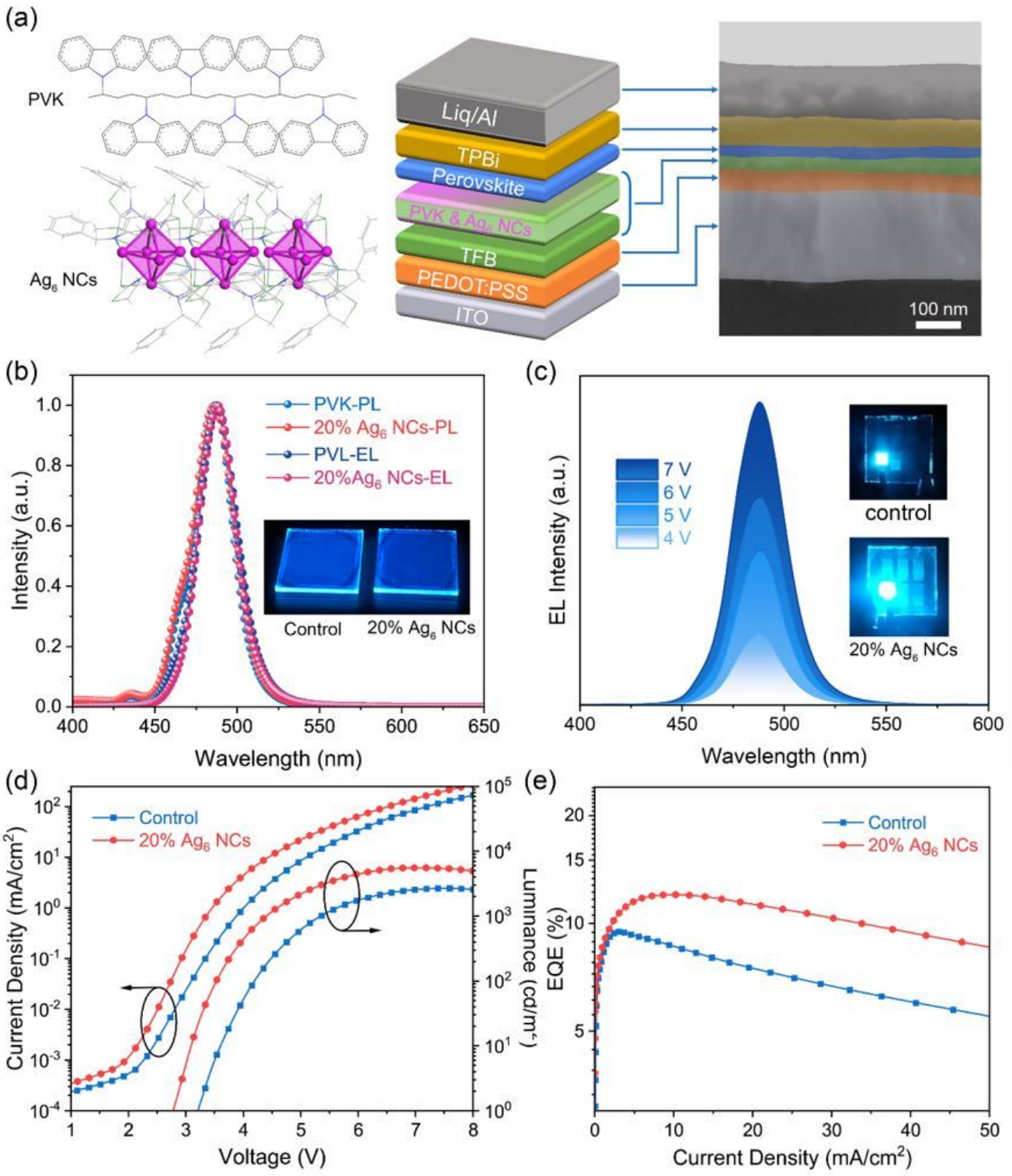

Figure 2

the molecule structure of the PVK and Ag_6 NCs, the schematic illustration and cross-sectional SEM images of p-i-n planar device structure (a), the normalized PL and EL spectra of the perovskite film and devices (b), the evolution of EL spectra under increasing bias voltage from 4 V to 7 V of the modified device (inset is a photo image of an operating PeLEDs) (c), the J-V-L curves (d) and EQE-J curves (e) of the control device and optimal device modified by 20% Ag_6 NCs.

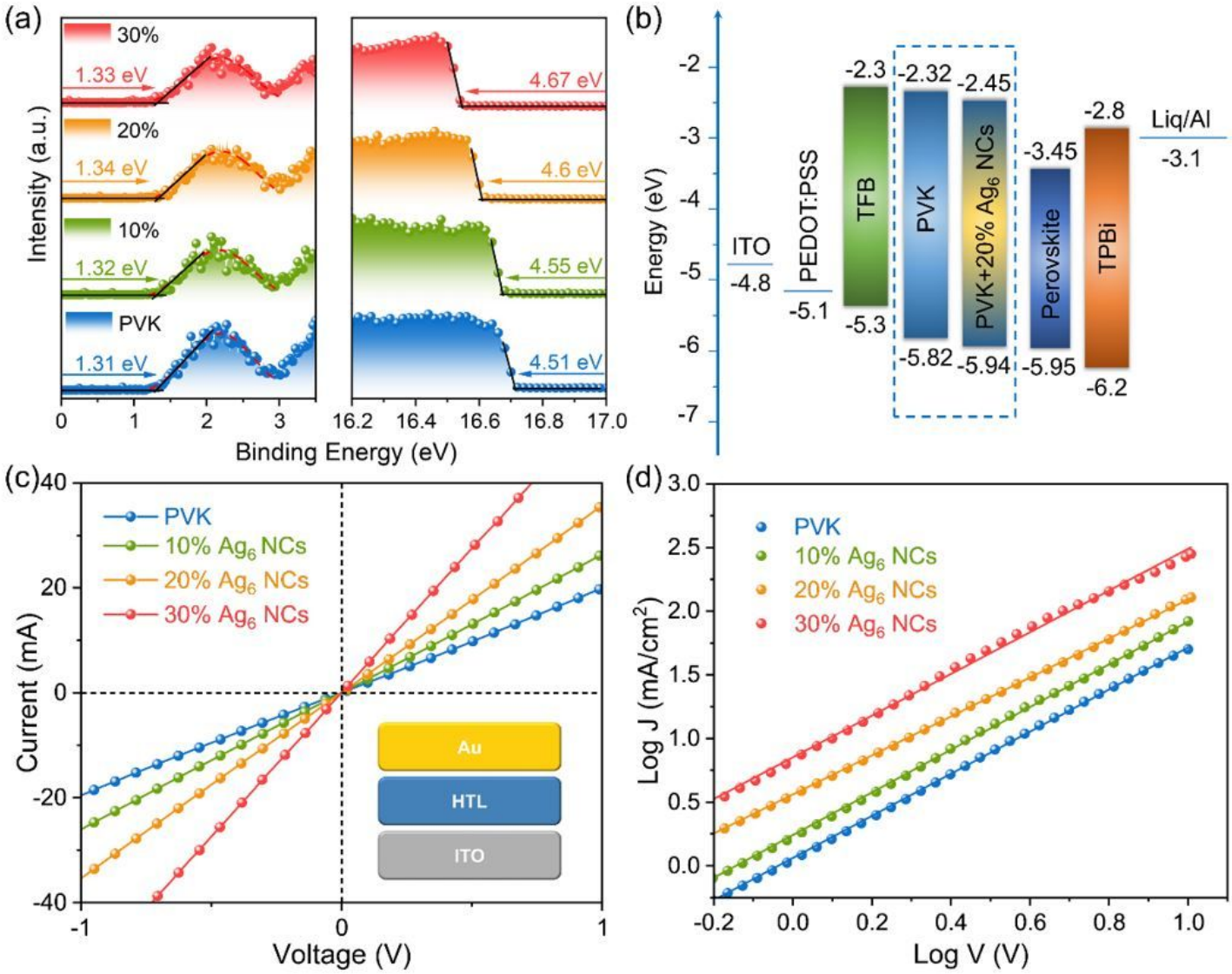

Figure 3

UPS spectra of the HTL (a), the energy of the materials (b), the current-voltage curves of capacitor-like devices (inset is the structure of the device) (c), and the J-V curves of the single-carrier device (d).

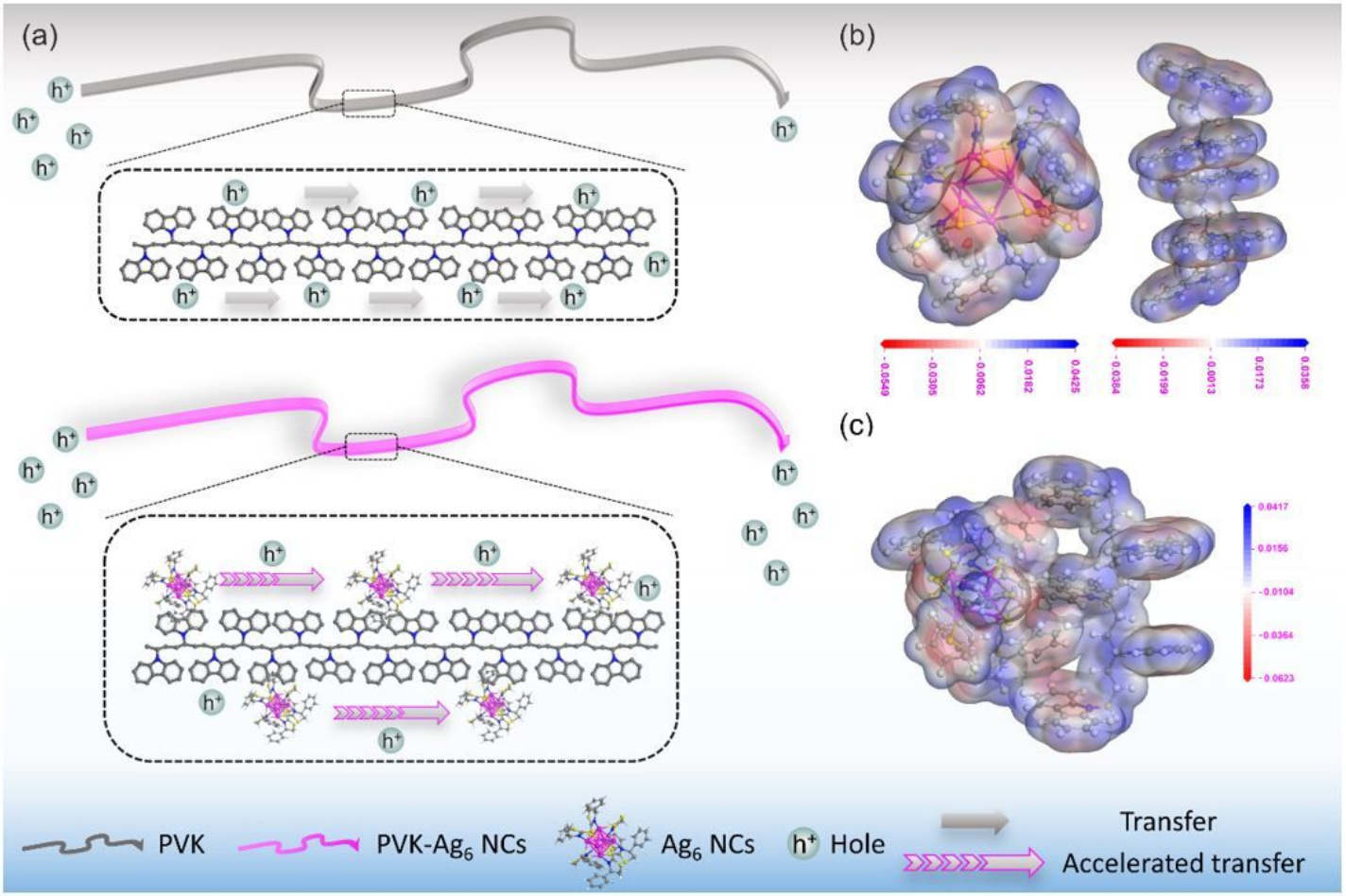

Figure 4

the hole transport and injection processes of PVK without and with Ag_6 NCs modifying (a), the electrostatic potentials of the PVK and the Ag_6 NCs (b), and the electronicstatic potentials of the mixed model of the PVK and Ag_6 NCs.

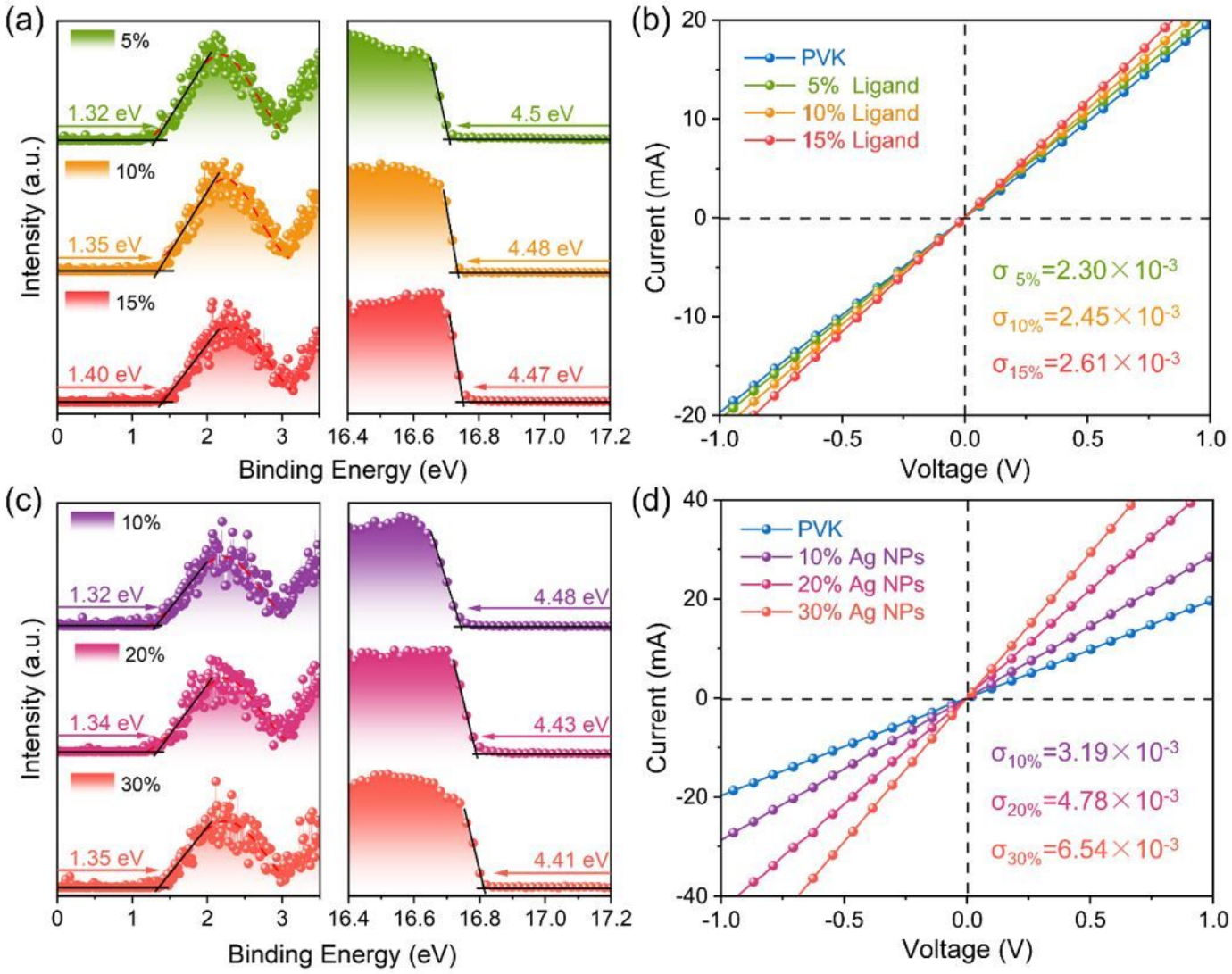

Figure 5

the UPS spectra (a), current-voltage curves of capacitor-like devices (b) with the different contents of ligands doping into PVK, the UPS spectra (c), and current-voltage curves of capacitor-like devices (d) with the different contents of Ag NPs doping into PVK.

Supplementary Files

This is a list of supplementary files associated with this preprint. Click to download.

- SupplementalMaterials.docx